Journal of the Indian Chemical Society 99 (2022) 100397

Contents lists available at ScienceDirect

Journal of the Indian Chemical Society

journal homepage: www.journals.elsevier.com/journal-of-the-indian-chemical-society

Crystal growth, structural, spectral, optical, DFT analysis and Z-scan analysis of pyridine-1-ium-2-carboxylatehydrogenbromide (PHBr) for optoelectronic and nonlinear optical applications

S. Priya [a,*], T. Umadevi [b], S. Gowri [a], G. Vinitha [c]

[a] PG Department of Physics, Cauvery College for Women(A), Affiliated to Bharathidasan University, Tiruchirappalli, 620 018, Tamil Nadu, India
[b] PG and Research Department of Physics, Periyar E.V.R College (A), Affiliated to Bharathidasan University, Tiruchirappalli, 620 023, Tamil Nadu, India
[c] Division of Physics, School of Advanced Sciences, Vellore Institute of Technology (VIT), Chennai, 600 127, India

ARTICLE INFO

Keywords:
Single crystal
Crystal structure
Hirshfeld surface analysis
Z-Scan
NLO
FT-IR

ABSTRACT

A single crystal of Pyridine-1-ium-2-carboxylatehydrogenbromide (PHBr) was grown using the Slow Evaporation Solution Technique. Using Single Crystal X-Ray Diffraction analysis, the crystal lattice characteristics and molecular structure of the grown crystal of PHBr were found and it corresponds to the Triclinic crystal system with space group Pi. Intra and intermolecular interactions were visualized using Hirshfeld surface analysis. The theoretical calculation conducted by Density Functional Theory (DFT) and it is well agreed with the experimental results. The Molecular optimized geometry, FT-IR and HOMO-LUMO energy gap were computed using the B3LYP level of theory with a 6-31 + G (d,p) basis set. The FT-IR spectrum studies are given here to look at the modes of vibration of numerous functional groups found in the PHBr crystal. The measurements of UV–visible NIR transmittance show that the crystal has a high transmittance over the whole visible spectrum. The Z-scan approach is used to perform third-order nonlinear optical (NLO) investigations on a PHBr crystal and optical properties such as linear and nonlinear refractive index are computed.

1. Introduction

Organic nonlinear optical (NLO) materials with functional interactions have gotten a lot of attention recently because of their multimodal laser-assisted device applications like optoelectronics, remote sensing, laser frequency shifting, laser printing, optical data storage, optical power limiting, optical signal processing and sensor protection [1–6].

Because of their greater molecular design flexibility, second and third harmonic generation efficiencies and applications in stabilizing fast fluctuations in terahertz wave generation, optical signal reshaping, laser power, laser reading modulation, high-resolution spectroscopy, ultrafast optical switching and two-photon laser scanning microscopy, organic crystalline materials break inorganic counterparts. Because of the presence of inter and intra-molecular hydrogen bonding between counter ions, this class of crystalline materials has high packing densities, an inherently fast response time, high thermal stability, a large bandgap, high optical thresholds for laser power and higher photochemical stabilities [7–13]. As a result, hydrogen bonding is the origin of non-covalent bond interactions, which provide a platform for crystal engineering supramolecular chemistry and chemical in the crystal's centrosymmetric system. Organic crystals with a centrosymmetric framework also exhibit second harmonic generation (SHG) and piezoelectric properties. Furthermore, optically active organic crystals with considerable third-order non linear optical properties will be important in future photonics technologies. Picolinic acid (pyridine 2-carboxylic acid) is commonly used in NLO research due to its ease of protonation in acid solution [14,15]. Due to the general strong complexation capacity of pyridine's nitrogen atom and carboxylate's oxygen atoms to various transition metal ions, Picolinic Acid has sparked considerable attention as a potential chelating ligand. Picolinic acid functions as a base, forming a compound containing a pyridine nitrogen atom. Picolinic acid is an essential biological component in the body that is created as a byproduct of tryptophan breakdown and it is also a pharmacologically active agent. The crystal structure, Hirshfeld surface analysis, FT-IR, and DFT/6-31 + G (d,p) level theory were used in this study to obtain the optimal geometry of Pyridine-1-ium-2-carboxylatehydrogenbromide, such as bond length

* Corresponding author.
E-mail address: priyaammu86@gmail.com (S. Priya).

https://doi.org/10.1016/j.jics.2022.100397
Received 14 December 2021; Received in revised form 16 February 2022; Accepted 22 February 2022
Available online 8 March 2022

and bond angle (PHBr). The UV–Vis spectrum was approximated using the TD-DFT/6-31G(d,p) basis set based on the optimized structure in the gas phase. The experimental optical, vibrational and NLO properties of the crystal have also been examined to establish its potential for NLO applications.

2. Experimental

Picolinic acid ($C_6H_6NO_2$) and hydrobromic acid (both of which have AR grade purity) were acquired from Sigma Aldrich. At the chosen saturation temperature, the various experimental solutions were created by combining an equimolar ratio of picolinic acid and hydrobromic acid salts. With continuous stirring, hydrobromic acid is carefully added to a homogeneous solution of picolinic acid (dissolved in double distilled water) until it is completely miscible and forms a homogeneous solution. To prevent the solvent from rapidly evaporating, the generated solution was filtered and coated with a perforated polythene sheet. The prepared solution was kept at a constant temperature in a water bath. Single crystal with dimensions of $10 \times 5 \times 4$ mm^3 was harvested after 12 days and the image of the as-grown crystal is shown below (Fig. 1). It was dried for 1 h in a hot air oven before being stored in an airtight container.

3. Characterization details

At room temperature, diffraction data from a single crystal of PHBr were collected using an Enraf Nonius CAD4-MV31 single-crystal X-ray diffractometer equipped with MoKα radiation (λ = 0.71073 Å). The PHBr crystal's UV–Visible spectra were measured using a SHIMADZU 1800 UV–Vis spectrometer in the 200–900 nm range. The Fourier Transform Infra-Red (FT-IR) spectrum was collected using the PerkinElmer FT-IR spectrometer in the range of 4000–400 cm^{-1} utilizing the KBr pellet approach to detect the distinct functional groups included in the PHBr crystal. The Z-scan method was used to calculate the third-order nonlinearity of a PHBr crystal with a 532 nm Semiconductor continuous wave laser as a laser source.

4. Crystallographic and computational details

SAINT [16] was utilized for data reduction and cell refinement in the structure of PHBr crystals. The crystal structure was solved directly with SHELXS-97 [17] and the refinement was done with SHELXL-97 [18]. PLATON [19,20] analysis demonstrated that the crystal structure included no solvent-accessible vacancies. Hirshfeld surface investigation was carried out using Crystal Explorer [21]. Quantum mechanical calculations utilizing the Becke3–Lee–Yang–Parr (B3LYP) functional enhanced with the standard B3LYP/6–31++G(d,p) basis set [22] were used to optimize the geometry and HOMO–LUMO using Gaussian-09 W [23] software. The Gaussview 05 program [24] was used to create visual presentations and check the normal mode assignments.

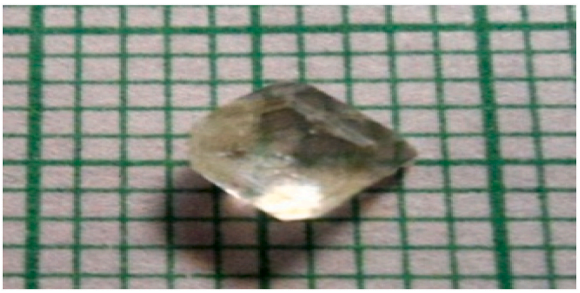

Fig. 1. As grown Crystal of PHBr.

5. Result & discussion

5.1. Single crystal X-ray diffraction studies

The crystalline and unit cell properties of the generated PHBr crystal were determined using X-ray diffraction analysis. According to single-crystal X-ray diffraction studies, PHBr crystallizes in a Triclinic system with lattice parameters a = 7.3182(13)Å, b = 7.3455(12)Å, c = 7.8061 (13)Å, α = 103.747(3) °, β = 92.298(4) °, γ = 116.387(3) °, and volume of the unit cell V = 359.98(11) $Å^3$. The space group Pī is centrosymmetric, which meets one of the essential and required material conditions for the NLO property of the material. PHBr has a density of 1.882 Mg/m^3 and Z = 2. The crystal data specifications, data collection settings, and reliability requirements are summarised in Table 1. Fig. 2a and b depict the molecular structure (ORTEP) of the grown PHBr crystal as well as the optimized PHBr structure. The packing diagram of PHBr is shown in Fig. 3. The hydrogen bonding statistics for PHBr are shown in Table 2. Intensity data were collected from all reflections and accurate unit cell parameters were obtained. A total of 5490 reflections were pooled for structure solution and refinement (1266 independent reflections, 1845 observed reflections, R_{int} = 0.2100). The corresponding transmission factors are 0.323 and 0.215. The Goodness of fit (S) of PHBr is 1.109. The CCDC number for the PHBr is 902759.

5.2. Hirshfeld surface analysis

Crystal Explorer Software was used to create the Hirshfeld surfaces analysis (HSs) and fingerprint plots for the PHBr molecule (FPs). Fig. 4 shows HSs plotted against d_{norm}, Curvedness and Shapeindex. The predominant interaction is intermolecular hydrogen bonding inside the Hirshfeld surface, as seen by the red patches. The hydrogen-bonding interactions between H and H play an important role in the molecular packing of this Schiff base. They account for 31.3% of the overall intermolecular interactions in the system under consideration. The Hirshfeld surface study also found a substantial amount of C–H interactions (8.2%). The surface's d_{norm}-colored spherical red patches convey hydrogen interactions with neighboring molecules. These red

Table 1
Crystal data and structure refinement.

CCDC Number	902759
Empirical formula	C_6 H_6 Br N O_2
Formula weight	204.03
Temperature	296(2) K
Wavelength	0.71073 Å
Crystal system	Triclinic
Space group	Pī
Unit cell dimensions	a = 7.3182(13) Å; α = 103.747(3)°. b = 7.3455(12) Å; β = 92.298(4)°. c = 7.8061(13) Å; γ = 116.387(3)°.
Volume	359.98(11) $Å^3$
Z	2
Density (calculated)	1.882 Mg/m^3
Absorption coefficient	5.643 mm^{-1}
F(000)	200
Crystal size	$10 \times 5 \times 4$ mm^3
Theta range for data collection	2.72–25.00°.
Index ranges	$-8 \le h <= 8$, $-8 \le k <= 4$, $-9 \le l <= 9$
Reflections collected	5490
Independent reflections	1266 [R(int) = 0.2100]
Completeness to theta = 25.00°	100.0%
Absorption correction	Semi-empirical from equivalents
Max. and min. transmission	0.323 and 0.215
Refinement method	Full-matrix least-squares on F^2
Data/restraints/parameters	1266/1/97
Goodness-of-fit on F^2	1.109
Final R indices [I > 2sigma(I)]	R1 = 6.2%, w*R*2 = 15.9%
R indices (all data)	R1 = 6.5%, w*R*2 = 16.1%
Extinction coefficient	0.056(11)
Largest diff. peak and hole	2.004 and −1.102 e.$Å^{-3}$

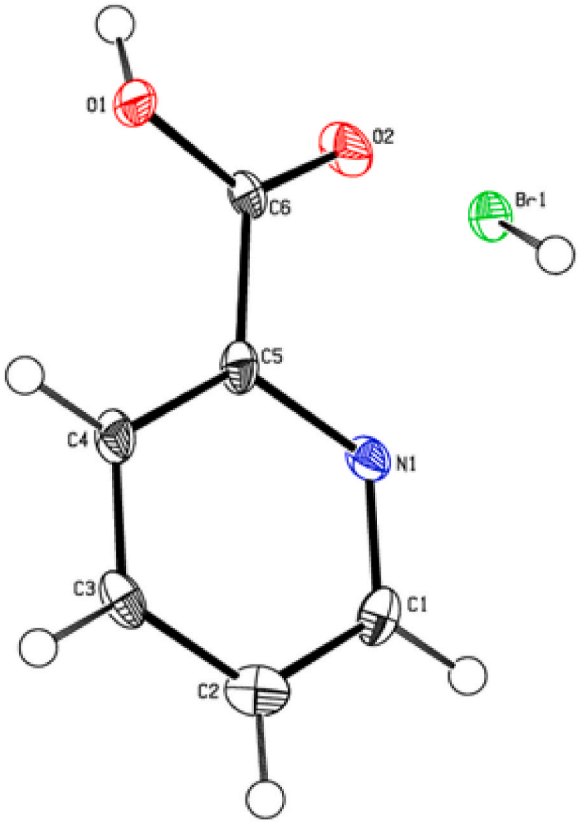

Fig. 2a. ORTEP diagram of PHBr.

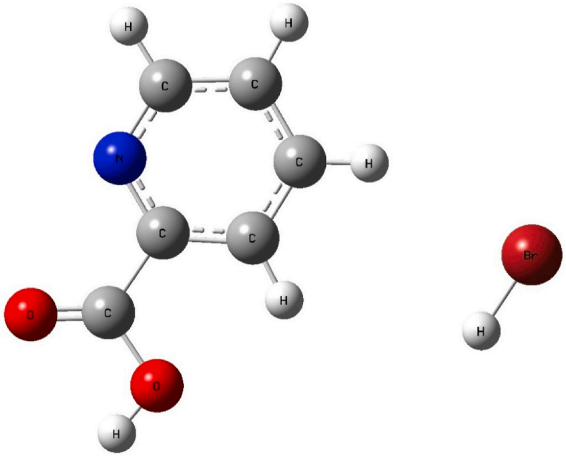

Fig. 2b. Optimized diagram of PHBr.

patches' surfaces are important because they provide intermolecular hydrogen bond interactions. All contact distances on the Hirshfeld surface may be represented as 2D fingerprint plots, the shapes of which are common in specific close-contact scenarios. Fingerprint plots, as illustrated in Fig. 5, are useful for distinguishing and comparing various types of interactions. Surface fingerprint plots revealed a high prevalence of H–H contacts. The surface is depicted as transparent to make the orientation and conformation of the functional groups visible. Other small contributions include interactions between H–Br (5.9%), N–Br (2.4%), C–C (2.2%), and N–O. (1.8%). The high percentages of H–H, H–O, and C–H contacts show that vdW and hydrogen bonding interactions are important in molecule packing, which is consistent with crystal packing structure.

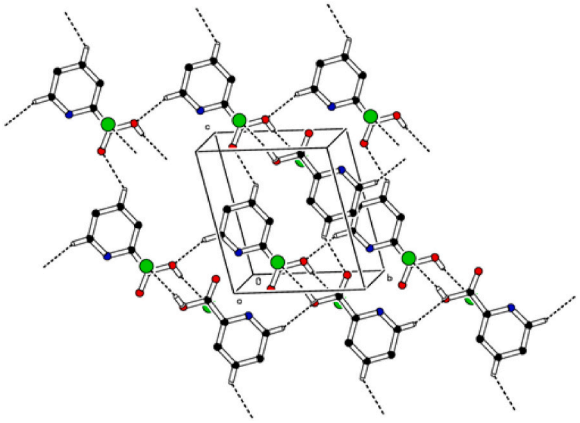

Fig. 3. Packing diagram of PHBr.

Table 2
Geometric details of hydrogen bond (Á).

Interactions	D-H	H … A	D … A	D-H … A	Symmetry
C3–H3···O2	0.93	2.40	3.122(8)	134	x,y,z+1
C1–H1A … O1	0.93	2.50	3.359(8)	154	x,y-1,z
O1–H1···Br1	0.82	2.34	3.133(5)	162	-x+1,-y+1,-z

5.3. Optimized geometry

According to B3LYP/6-31 + G(d,p) simulations, the optimized PHBr molecule is near the geometry in the solid phase. Geometric parameter calculation is effective, according to Foresman and Frisch, if the difference in bond length between calculated and experimental values is less than 0.01–0.02° and the divergence of bond angle and torsion angle is less than 1-2° [25,26]. The best structure with the atom counts and geometric properties chosen is shown in Fig. 2b and Table 3. The total divergence between calculated (gas phase) and experimental (solid phase) bond length values in the current examination of PHBr crystal is in the range of 0.060 and 0.010 at HF and DFT basis set, respectively, while bond angle values are in the range of 0.05° at HF and 0.516° at DFT level. As a result, the C1–C2 and C3–C4 ring bond lengths for the PHBr molecule with sp2 hybridization were determined to be 1.38 Å and 1.385 Å, respectively. For HF, the computational values assigned to C1–C2 and C3–C4 is 1.39 Å and 1.38 Å, respectively; for DFT, the values are 1.4 Å and 1.39 Å. The PHBr molecule's C3–C4 and C4–C5 bond lengths, on the other hand, are expected to be 1.38 Å and 1.361 Å, respectively. Furthermore, the Br1–H1, O1–C6, and O2–C6 bond lengths of the PHBr molecule are determined to be 1.41 Å, 1.33 Å, and 1.209 Å, respectively. The lengths of the N1–C1 and N1–C5 bonds in the PHBr molecule's ring are estimated to be 1.336 Å and 1.354 Å, respectively. The C1–C2–C3 and C3–C4–C5 ring angles for the PHBr molecule have been determined to be 118.4° and 119.5°, respectively, as anticipated given the sp2 hybridization of the core atoms. There is no variation in the O1–C6 bond length or the C1–C2–C3 bond angle. The N1–C1–C2 bond angle has a maximum deviation of 2.93° at HF and 3.23° at the DFT level.

5.4. Molecular electrostatic potential

The molecular electrostatic potential (MEP) is commonly used to predict compounds' electrophilic and nucleophilic active sites. It is based on the fact that the positive region of the MEP on one molecular surface tends to interact with the negative region of another molecule, and the stronger the tendency, the more positive the positive, the more negative the negative value. The surface local minima (maxima) of ESP are shown by the red (blue) area, while the maximum (minimum) values

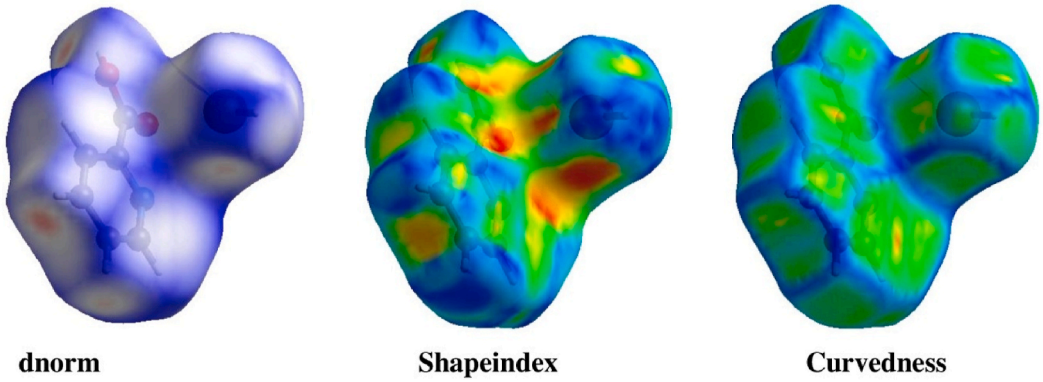

Fig. 4. dnorm, shapeindex, curvedness diagram of PHBr.

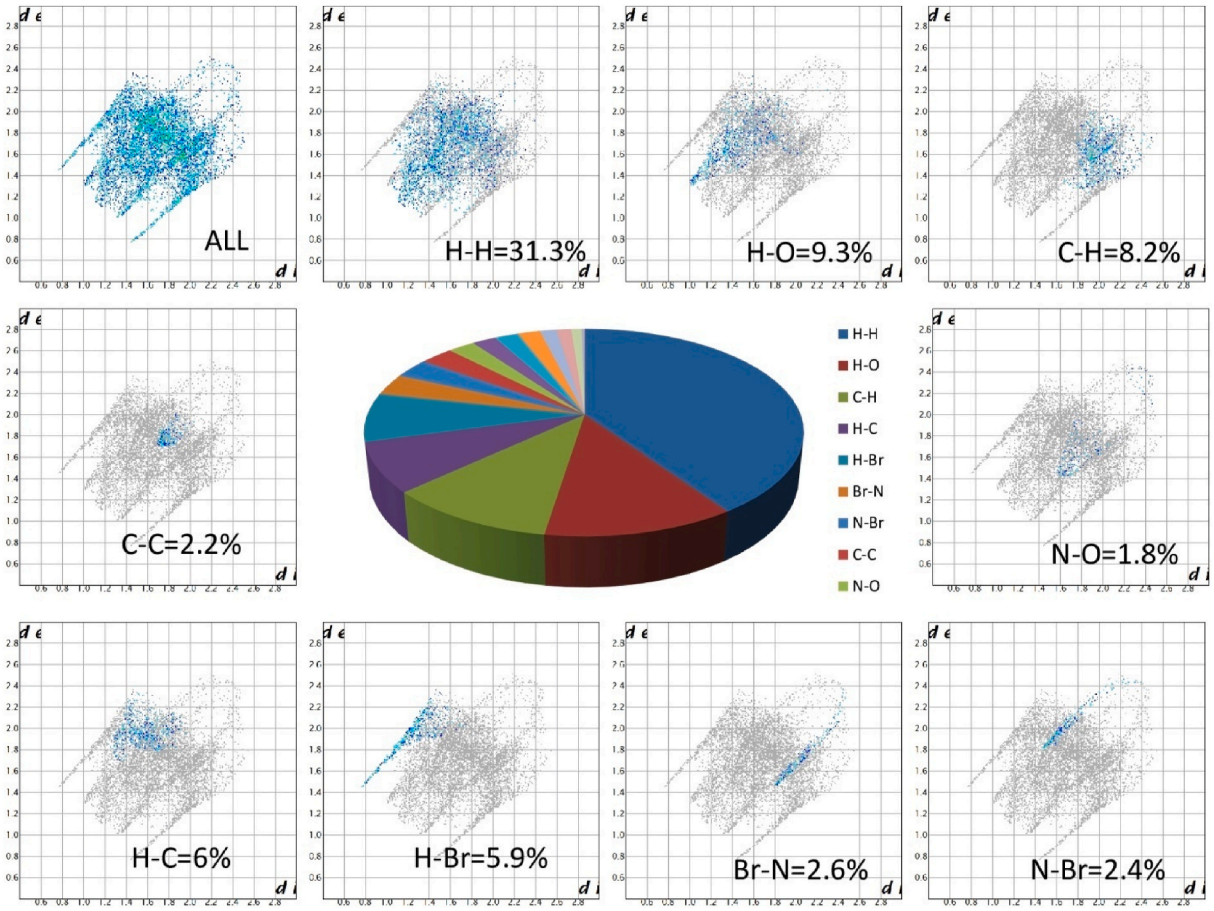

Fig. 5. 2D fingerprint plot of PHBr.

are represented by the orange (cyan) beads on the molecular surface. The negative (red) parts of MEP were linked with electrophilic reactivity, whereas the positive (blue) regions were connected with nucleophilic reactivity. The Molecular Electrostatic Potential (MEP) is related to the electrical density and is a useful descriptor for identifying electrophilic attacks, nucleophilic reactions, and hydrogen-bonding interactions [27]. The MEP of PHBr is shown in Fig. 6. Atoms in the PHBr molecule must have either a positive or a negative potential isosurface. The PHBr MEP clearly shows that H in O1 and H in Br1 have positive potential isosurface centres. At PHBr, the extreme limits of electron density are -7.010×10^{-2} (red) and $+7.010 \times 10^{-2}$ (blue).

5.5. Vibration assignment

The vibrational modes of a semi-organic crystal are linked to the electrical properties of nonlinear optical material, such as first and second-order polarizabilities. These properties are linked with molecular structure and spectrum intensities because they represent vibrational polarizabilities, the magnitudes of which are tied to electronic polarizabilities [28]. Fig. 7 depicts a comparison between theoretical and experimental FT-IR. Table 4 shows the theoretical and experimental vibrational wavenumbers of the PHBr crystal derived using B3LYP/6-31 + G(d,p).

Table 3
Optimized Geometrical values of PHBr (Å).

Atoms	Bond length(Å)	HF	DFT
Br1–H1	1.41(2)	1.401	1.42
O1–C6	1.333(8)	1.333	1.364
O2–C6	1.209(8)	1.838	1.208
N1–C1	1.336(9)	1.314	1.334
N1–C5	1.354(8)	1.3222	1.341
C1–C2	1.380(10)	1.39	1.4
C2–C3	1.390(10)	1.38	1.393
C3–C4	1.385(10)	1.387	1.395
C4–C5	1.361(10)	1.386	1.4
C5–C6	1.492(10)	1.503	1.503
Atoms	**Bond angle(°)**	**HF**	**DFT**
C1–N1–C5	122.1(6)	120.24	117.58
N1–C1–C2	120.3(6)	123.23	123.53
C1–C2–C3	118.4(7)	118.44	118.56
C4–C3–C2	120.0(6)	118.54	118.48
C5–C4–C3	119.5(6)	118.22	118.54
N1–C5–C4	119.7(6)	120.31	123.88
N1–C5–C6	114.5(6)	115.51	115.42
C4–C5–C6	125.7(6)	123.17	118.54
O2–C6–O1	126.0(6)	125.29	122.2
O2–C6–C5	121.6(6)	124.35	125.89
O1–C6–C5	112.4(5)	112.34	111.9

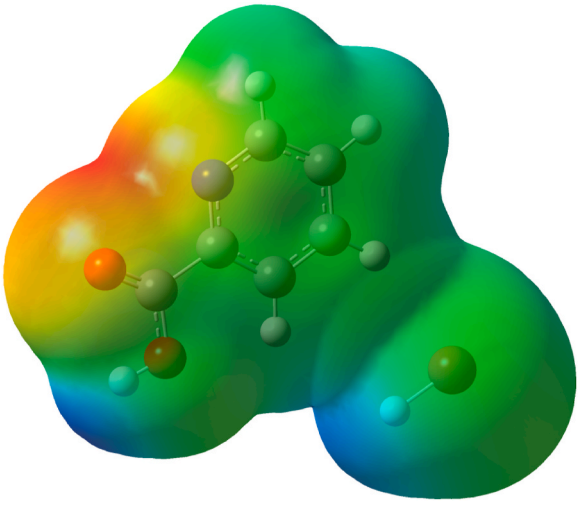

Fig. 6. MEP of PHBr.

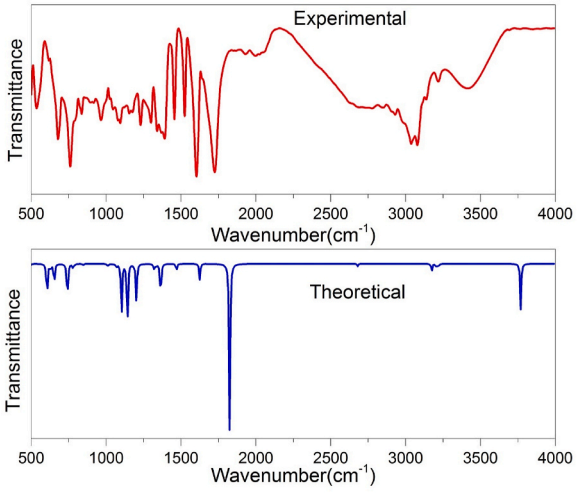

Fig. 7. Experimental and theoretical FT-IR spectrum of PHBr.

5.5.1. C–H vibrations

The heteroaromatic organic compounds exhibit a medium band in the range 3100–3000 cm^{-1} due to the C–H stretching vibrations; the band is visible in this PHBr crystal at 3140 cm^{-1}. In-plane ring C–H bending vibrations are frequently seen as low-intensity, sharp bands in the 1300–1000 cm^{-1} range [29]. In the FT-IR spectra of PHBr, a band at 3140 cm^{-1} may be ascribed to C–H stretching vibration. B3LYP/6-31 + G (d, p) are used to determine the theoretically measured vibrations of 3154 cm^{-1}.

5.5.2. C–C vibrations

Ring vibrations (C═C) are prominent in the pyridine derivative spectrum and have a strong influence on the specific region of the heteroaromatic ring vibrations [30]. C═C stretching modes are attributed largely to the bands found in pyridine derivatives in the 1500-1600 cm^{-1} region [31]. Due to the absence of aromaticity in the present molecule, the homogeneous C ….C vibrations are divided into C═C and C–C stretching vibrations. At 1460 cm^{-1}, C═C stretching vibrations have been observed. PHBr was discovered in the experimental FTIR spectra at 1460 cm^{-1} and C–C stretching vibration. B3LYP/6-31 + G(d, p) calculates the putative C–C stretching mode at 1469 cm^{-1}.

5.5.3. O–H vibrations

Stretching, inplane bending and out-of-plane bending are all generated by the O–H group. Because the vibrations in the O–H group are the most sensitive to the environment, they show the most substantial changes in the spectra of the hydrogen-bonded species. The substantial absorption at 3769 cm^{-1} in the FT-IR spectrum is caused by the O–H stretching vibration, which is connected to intermolecular hydrogen bonding. The O–H vibration is assigned the estimated value at 3768 cm^{-1} in the B3LYP/6-31 + G (d,p) technique.

5.5.4. Aromatic C–H vibration

The vibrational frequencies of the C–H out-of-plane bending modes are mostly governed by the number of neighboring hydrogen atoms on the ring and the kind of substituent on the pyridine ring. C–H out of plane bending modes have a medium to moderate intensity and occur in the 950–600 cm^{-1} range [32]. In-plane aromatic C–H deformation vibrations occur in the range 1300–1000 cm^{-1}, however, the band occurs at 1148 cm^{-1} in this example. B3LYP/6-31 + G(d,p) calculates the putative C–H stretching mode at 1149 cm^{-1}. The C–H out-of-plane deformation band, which is a characteristic feature of o-substituted pyridines, is responsible for the substantial absorption at 926 cm^{-1} [33]. B3LYP/6-31 + G (d,p) measured the calculated value at 922 cm^{-1}.

5.6. HOMO-LUMO analysis

The expected HOMO energies are −0.07552 eV, while the determined LUMO energies are −0.27735 eV. The energy difference between HOMO and LUMO not only determines a molecule's chemical stability but also influences molecular electrical transport capacities. The HOMO-LUMO energy gap for the PHBr molecule was determined to be 5.4921eV. Absolute hardness and absolute electronegativity may be calculated using HOMO and LUMO energies [34,35]. The value of various systems corresponds to empirically determined chemical softness and hardness [36]. Ionization potential and electron affinity values are used to calculate significant variables such as global hardness, chemical potential, and global electrophilicity index. The values are 0.100915 eV, 0.17643 eV, and 0.15235 eV, respectively. Fig. 8 depicts the HOMO-LUMO energy gap.

5.7. UV–vis spectrum analysis

The absorption peaks' wavelengths are obtained from the UV–Visible spectrum. The electronic absorption spectrum of the PHBr molecule was computed using the Time Dependent Density Functional Theory (TD-

Table 4
Theoretical and Experimental vibrational wavenumbers (cm^{-1}) of PHBr crystal calculated by B3LYP/6-31 + G(d,p).

S.No	IR	Freq.	Red. masses	Frc consts	IR Inten	Raman Activ	Depolar (P)	Depolar (U)
1	–	26	10.2057	0.0041	0.9517	0.1541	0.7487	0.8563
2	–	37	12.3122	0.0099	2.4077	1.6916	0.75	0.8571
3	–	58	9.1096	0.0178	0.8514	0.4405	0.5899	0.742
4	–	86	4.6706	0.0203	1.0014	3.4028	0.75	0.8571
5	–	125	1.1718	0.0109	11.711	1.3437	0.75	0.8571
6	–	166	3.0091	0.049	9.0688	1.0533	0.75	0.8571
7	–	182	1.0294	0.0201	36.914	2.7922	0.7296	0.8436
8	–	225	6.0084	0.1789	1.0216	0.3659	0.7286	0.843
9	–	390	8.86	0.7936	3.978	3.4908	0.2721	0.4278
10	428	431	2.6599	0.2908	11.478	0.1864	0.75	0.8571
11	494	492	7.7393	1.105	3.1712	0.9022	0.5966	0.7473
12	–	497	3.2714	0.4759	1.6742	0.4416	0.75	0.8571
13	611	605	1.2822	0.2763	79.322	2.4289	0.75	0.8571
14	–	628	6.8494	1.592	12.435	5.6733	0.7108	0.831
15	–	653	4.8372	1.2145	48.726	1.3669	0.0931	0.1704
16	–	740	2.3546	0.7607	88.449	0.049	0.75	0.8571
17	–	775	1.7952	0.6358	7.2106	0.0787	0.75	0.8571
18	–	787	5.1922	1.8958	4.203	14.4301	0.1273	0.2258
19	–	847	3.1142	1.3151	2.991	1.3208	0.75	0.8571
20	922	926	1.3478	0.6806	0.1349	0.135	0.75	0.8571
21	998	997	1.4616	0.8558	0.2389	0.0865	0.75	0.8571
22	–	1012	7.2576	4.3798	6.0628	25.5092	0.0593	0.1119
23	1046	1050	1.4542	0.9446	0.0074	0.2657	0.75	0.8571
24	–	1069	2.6686	1.7966	6.93	24.8948	0.0449	0.086
25	–	1102	2.2009	1.5755	111.33	1.5076	0.5956	0.7465
26	1148	1141	2.1813	1.6741	148.89	3.4897	0.5781	0.7327
27	1180	1184	1.1391	0.941	1.9389	10.4512	0.1811	0.3066
28	–	1202	1.9866	1.6906	86.914	29.052	0.2365	0.3825
29	–	1318	2.7575	2.8219	11.767	4.003	0.2822	0.4402
30	1335	1332	2.0493	2.1418	6.9848	1.034	0.518	0.6825
31	1363	1364	2.7626	3.0277	83.656	11.5212	0.2698	0.425
32	1460	1469	2.0807	2.6459	16.245	5.1426	0.3015	0.4633
33	–	1506	2.3264	3.1094	0.3929	2.819	0.6948	0.8199
34	–	1625	5.5673	8.657	31.724	5.0786	0.5319	0.6944
35	–	1629	5.7233	8.9525	2.0925	71.0748	0.5472	0.7073
36	–	1825	10.399	20.406	350.12	99.7229	0.2609	0.4139
37	–	2680	1.0205	4.3179	5.4323	88.8475	0.2202	0.361
38	3140	3154	1.0895	6.4678	15.816	119.008	0.395	0.5663
39	–	3204	1.0913	6.6012	8.5598	135.355	0.5155	0.6803
40	3216	3220	1.0934	6.6782	6.8944	187.425	0.2223	0.3638
41	3222	3236	1.0944	6.7513	0.5982	165.821	0.1909	0.3205
42	3768	3769	1.0647	8.9095	93.843	139.466	0.2609	0.4138

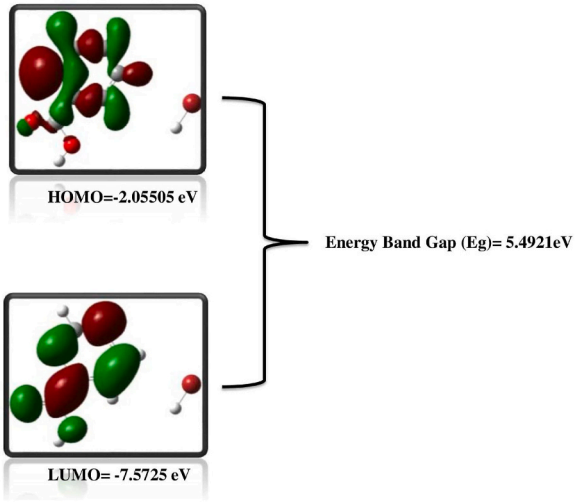

Fig. 8. HOMO-LUMO energy gap of PHBr.

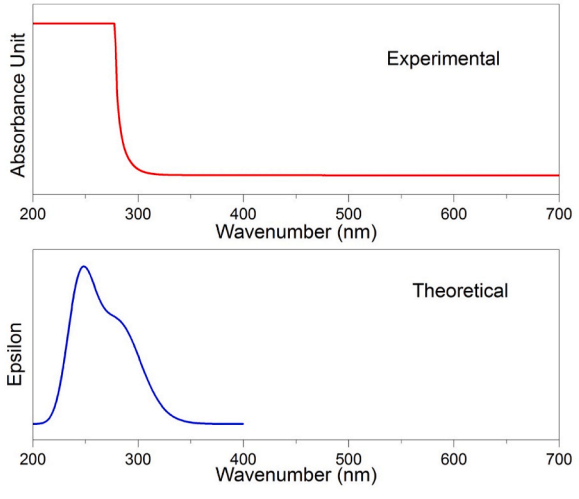

Fig. 9. Observed and calculated UV–Vis spectra of the PHBr molecule.

DFT) approach using basis set 6-31G(d,p) to investigate its absorption features. The measured and computed UV–Vis spectra of the PHBr molecule are shown in Fig. 9. Absorption wavelengths and oscillator strengths of 284.87 nm, 0.0014, and 246.51, 0.0223, respectively, are among the electronic properties of the PHBr molecule. The maximum experimentally recorded absorption levels are 270 nm.

5.8. Z scan

The Z-scan technique is a dependable method for identifying nonlinear optical properties of materials such as nonlinear absorption and nonlinear refraction. The method has been developed for several applications such as optical limiting [37], multi-photon polymerization [38], and optical switching [39]. Stryland and Sheik-Bahae [40] developed the Z-scan method. The sample was moved in the same direction as the laser beam's propagation from the negative (– Z) to the positive (+Z) axis. The intensity of a laser beam is related to the refractive index and absorption type of the material. A closed aperture is used to measure the nonlinear refractive index, whereas an open aperture is used to measure nonlinear absorption. This configuration is powered by the Kerr effect in nonlinear optics. Figs. 10 and 11 show the PHBr crystal's obtained open and closed aperture spectra. The sample causes additional focusing or defocusing depending on the nonlinear refraction levels. The PHBr crystal is held in a quartz cell. The sign of the nonlinear phase shift determines the position of the peak and valley relative to the z-axis. The difference in normalized transmittance between the peak and valley may be used to compute the phase shift size. The specifics of the computation are as follows.

$$\Delta T_{p-v} = 0.406\ (1-S)^{0.25}\ |\varphi| \tag{1}$$

where S is the aperture linear transmittance and is calculated using the following equation

$$S = 1 - exp\left(-2\ r_a^2 / \omega_a^2\right) \tag{2}$$

where $r_a$is the radius of the aperture and ω_a is the beam radius at the aperture, the non-linear refractive index is given by the relation

$$n_2 = \varphi / KI_0 L_{eff} \tag{3}$$

where $K = 2\pi/\lambda$ (where λ is the laser wavelength).

I_0 is the input intensity, ($Z = 0$, $L_{eff} = [1\text{-}exp(-\alpha L)]/\alpha$ is the effective thickness of the sample and α is the linear absorption coefficient of the PHBr crystal. From the open aperture Z – scan data, the non-linear absorption coefficient is estimated as

$$\beta = 2\sqrt{2}\Delta T / I0Leff \tag{4}$$

where Δ T is the one valley at the open aperture Z-scan curve.

The value of absorption co-efficient β will be negative for saturable absorption and positive for two-photon absorption. The real and imaginary parts of the third-order non-linear optical susceptibility χ^3 are defined as equation

$$Re\,\chi^3(esu) = 10^{-4}\left(\varepsilon_0 C^2 n_0^2 n_2\right) / \pi\ \left(Cm^2 / W\right) \tag{5}$$

$$Im\,\chi^3(esu) = 10^{-2}\left(\varepsilon_0 C^2 n_0^2 \lambda\beta\right) / 4\pi^2\ (Cm / W) \tag{6}$$

In our experiment for PHBr crystal non linear refractive index $n_2 = 4.2552 \times 10^{-9}(cm^2/W)$. The absorption co-efficient β calculated from open aperture normalized transmittance was obtained to $\beta = 3.8835 \times 10^{-4}(cm/W)$. According to the equation by (5) & (6), this value of n_2 & β can be used to calculate χ^3. The calculated χ^3 value is 4.88×10^{-6} esu.

6. Conclusion

An organic nonlinear optical Pyridine-1-ium-2-carboxylatehydrogenbromide (PHBr) single crystal with new third-order NLO properties was successfully synthesized at room temperature. According to the crystal lattice properties derived from single-crystal X-ray diffraction analysis, PHBr belongs to the triclinic crystal system with the space group of $P\bar{1}$. The calculated molecule structural geometry, such as bond length and bond angle, matches well with the experimental data. The presence of various functional groups and their vibrational assignments were detected using FT-IR and compared to DFT analysis. Hirshfeld's surface study of PHBr crystal reveals intermolecular interactions in the crystalline form. The fingerprint 2D graphs confirm the percentage of contact in the PHBr molecule. Using the Z-scan approach, the nonlinear saturable absorption coefficient and self-defocusing nature of the PHBr crystal were calculated, and these properties were proven to increase the optical limiting applications of this material.

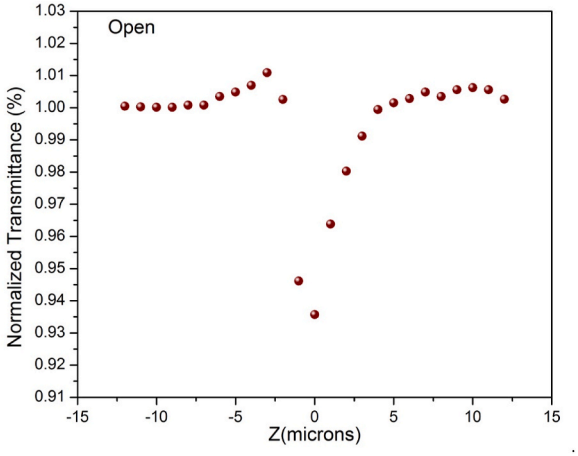

Fig. 10. Open aperture of PHBr.

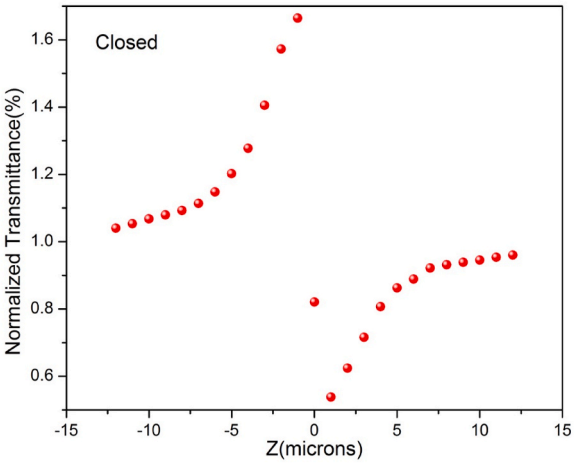

Fig. 11. Closed aperture of PHBr.

Declaration of interests

I declare that I have no known competing financial interests or personal relationships that could have appeared to influence the work reported in this paper.

References

[1] K. Arunkumar, S. Kalainathan, Synthesis, growth and characterization of organic nonlinear optical single crystal 1,3-bis (4-methoxyphenyl) prop-2-en-1-one (BMP) by vertical Bridgman technique, Optic Laser. Technol. 89 (2017) 143–150, https://doi.org/10.1016/j.optlastec.2016.10.003.

[2] B. Babu, J. Chandrasekaran, B. Mohanbabu, Y. Matsushita, M. Saravanakumar, Growth, physicochemical and quantum chemical investigations on 2-amino 5-chloropyridinium 4-carboxybutanoate-an organic crystal for biological and optoelectronic device applications, RSC Adv. 6 (2016) 110884–110897, https://doi.org/10.1039/C6RA15791B.

[3] K. Parasuraman, K. SakthiMurugesan, R. UthraKumar, S. Jerome Das, B. Milton Boaz, Growth, optical, mechanical and dielectric studies on NLO active pure and

metal ion doped single crystals of bis-thiourea Zinc chloride, Physica B 406 (2011) 3856–3860, https://doi.org/10.1016/j.physb.2011.07.011.
[4] Q.M.A. Hassan, Two-photon absorption-based optical limiting in 2-(2-methoxybenzyllideneamino)-5-methylphenylmercuric chloride-doped PMMA film, Mod. Phys. Lett. B 28 (2014), https://doi.org/10.1142/S0217984914500791,1450079-14500898.
[5] S. Karthigha, C. Krishnamoorthi, Synthesis, growth, crystal structure, optical and third order nonlinear optical properties of quinolinium derivative single crystal: PNQI, J. Phys. Chem. Solid. 114 (2018) 133–140, https://doi.org/10.1016/j.jpcs.2017.10.043.
[6] D.S. Chemla, J. Zyss, Nonlinear Optical Properties of Organic Molecules and Crystals, first ed., vol. 1, Academic Press, New York, 1987.
[7] S. Karthick, K. Thirupugalmani, G. Shanmugam, V. Kannan, S. Brahadeeswaran, Experimental and quantum chemical studies on N-H—O hydrogen bonded helical chain type Morpholinium 2-Chloro-4-Nitrobenzoate: a phasematchable organic nonlinear optical material, J. Mol. Struct. 1156 (2018) 264–272, https://doi.org/10.1016/j.molstruc.2017.11.115.
[8] K. Nivetha, W. Madhuri, Structural, spectral, thermal, and optical studies of stilbazolium derivative crystal: (E)-4-(3-hydroxy-4-methoxystyryl)-1-methyl pyridinium iodide monohydrate, Opt Laser. Technol. 109 (2019) 496–503, https://doi.org/10.1016/j.optlastec.2018.08.035.
[9] K. Senthil, S. Kalainathan, Y. Kondo, F. Hamada, M. Yamada, Investigation on the crystal growth, molecular structure and nonlinear optical susceptibilities of 2-[2-(4-Ethoxy-phenyl) vinyl]-1-ethyl-stilbazolium iodide (EESI) by Z-scan technique using He–Ne laser for third-order nonlinear optical applications, Optic Laser. Technol. 90 (2017) 242–251, https://doi.org/10.1016/j.optlastec.2016.10.019.
[10] P. Nagapandiselvi, C. Baby, R. Gopalakrishnan, Self-assembled supramolecular structure of N,N,N0,N0 -tetramethylethylenediammonium-bis- (4-nitrophenolate): synthesis, single crystal growth and photo physical properties, RSC Adv. 4 (2014) 22350–22358, https://doi.org/10.1039/C4RA02393E.
[11] K. Nivetha, S. Kalainathan, A new nonlinear optical stilbazolium family crystal of (E)-1-ethyl-2-(4-nitrostyryl) pyridin-1-ium iodide: synthesis, crystal structure and its third-order nonlinear optical properties, J. Phys. Chem. C 122 (2018) 4572–4582, https://doi.org/10.1021/acs.jpcc.7b11884.
[12] Harsh Yadav, Nidhi Sinha, Binay Kumar NidhiTyagi, Enhancement of optical, piezoelectric and mechanical properties in crystal violet dye doped benzophenone crystal grown by Czochralski technique, Cryst. Growth Des. 15 (2015) 4908–4917, https://doi.org/10.1021/acs.cgd.5b00792.
[13] M. Hasmuddin, M.M. Abdullah, Preeti Singh, M. Shkir, N. Vijayan, M.A. Wahab, Ab-initio study of L-Tartaric Acid (LTA) single crystal for NLO application, Optic Laser. Technol. 74 (2015) 53–59, https://doi.org/10.1016/j.optlastec.2015.05.013.
[14] G. Peramaiyan, P. Pandi, B.M. Sornamurthy, G. Bhagavannarayana, R. Mohan Kumar, Spectrochim. Acta A 95 (2012) 310–316.
[15] S. Gowri, K. Anitha, A. Suresh, T. Uma Devi, S. Selvanayagam, D. Sajan, A. Chandramohan, N. Lawrence, Spectrochim. Acta 95 (2012) 73–79.
[16] SAINT Plus (v 6.14), Bruker AXS Inc., Madison, WI, 2008.
[17] G.M. Sheldrick, Acta Crystallogr. A 64 (2008) 112–122.
[18] G.M. Sheldrick, Acta Crystallogr. C 71 (2015) 3–8.
[19] A.L. Spek, PLATON, A Multipurpose Crystallographic Tool, Utrecht University, Utrecht, Netherland, 2002.
[20] A.L. Spek, J. Appl. Crystallogr. 36 (2003) 7–13.
[21] S.K. Wolff, D.J. Grimwood, J.J. McKinnon, D. Jayatilaka, M.A. Spackman, M. A, CrystalExplorer1.5, vol. 2005, University of Western Australia, 2005.
[22] H.B. Schlegel, J. Comput. Chem. 3 (1982) 214–218.
[23] M.J. Frisch, et al., Gaussian-09, Revision A.01, Gaussian, Inc., Wallingford, CT, 2009.
[24] R. Dennington, T. Keith, J. Millam, GaussView, Version 5, Semichem Inc., Shawnee Mission, KS, 2009.
[25] J.B. Foresman, E. Frisch, Exploring Chemistry with Electronic Structure Methods, Gaussian, Inc., Pittsburgh, PA, 1996.
[26] M.P. Andersson, P. Uvdal, New scale factors for harmonic vibrational frequencies using the B3LYP density functional method with the triple-ζ basis set 6-311+G(d,p), J. Phys. Chem. A 109 (2005) 2937–2941.
[27] B. Champagne, B. Kirtman, Vibrational versus electronic first hyperpolarizabilities of π-conjugated organic molecules: an ab initio Hartree–Fock investigation upon the effects of the nature of the linker, Chem. Phys. 245 (1999) 213–226, https://doi.org/10.1016/S0301-0104(99)00072-5.
[28] R.N. Singh, SangeetaSahu PoonamRawat, Investigation of spectroscopic, structural and non-linear optical properties of ethyl 3,5-dimethyl-4-[(benzenesulfonyl)-hydrazonoethyl]-1H-pyrrol-2-carboxylate, J. Mol. Struct. 1054–1055 (2013) 123–133, https://doi.org/10.1016/j.molstruc.2013.09.016.
[29] S. Muthu, S. Renuga, Vibrational and spectroscopic investigation on the structure of 5H-dibenzo[b,f]azipine-5-carboxamide, Spectrochim. Acta A 114 (2013) 1–10, https://doi.org/10.1016/j.saa.2013.05.004.
[30] S. Ramalingam, S. Periandy, S. Mohan, Vibrational spectroscopy (FTIR and FTRaman) investigation using ab initio (HF) and DFT (B3LYP and B3PW91) analysis on the structure of 2-amino pyridine, Spectrochim. Acta A 77 (2010) 73–81, https://doi.org/10.1016/j.saa.2010.04.027.
[31] Z. Dega-Szafran, M. Jaskólski, M. Szafran, OHO hydrogen bond and electrostatic interactions in a complex of pyridine betaine with phenylacetic acid studied by X-ray diffraction, FTIR spectroscopy and PM3, DFT calculations, J. Mol. Struct. 555 (2000) 191–201, https://doi.org/10.1016/S0022-2860(00)00602-5.
[32] A. Jayarama, H.J. Ravindra, Anthoni Praveen Menezes, S.M. Dharmaprakash, SeikWeng Ng, Synthesis, growth, and characterization of 3-(4-Methoxyphenyl)-1-(pyridin-2-yl) prop-2-en-1-one single crystal: a potential NLO material, J. Mol. Struct. 1051 (2013) 285–291, https://doi.org/10.1016/j.molstruc.2013.08.026.
[33] I. Bryndal, E. Kucharska, W. Sąsiadek, M. Wandas, T. Lis, J. Lorenc, J. Hanuza, Molecular and crystal structures, vibrational studies and quantum chemical calculations of 3 and 5-nitroderivatives of 2-amino-4-methylpyridine, Spectrochim. Acta A 96 (2012) 952–962, https://doi.org/10.1016/j.saa.2012.07.121.
[34] R.G. Parr, R.A. Donnelly, M. Levy, W.E. Palke, Electronegativity: the density functional viewpoint, J. Chem. Phys. 68 (8) (Apr. 1978) 3801–3807.
[35] R.G. Parr, R.G. Pearson, Absolute hardness: companion parameter to absolute electronegativity, J. Am. Chem. Soc. 105 (1983) 7512–7516.
[36] R. Pearson, Hard and soft acids and bases, J. Am. Chem. Soc. 85 (1963) 3533–3539.
[37] E. Van Stryland, H. Vanherzeele, M. Woodall, M. Soileau, A. Smirl, S. Guha, Opt. Eng. 24 (1985) 613–623.
[38] C. Mendonca, D. Correa, F. Marlow, T. Voss, P. Tayalia, E. Mazur, Appl. Phys. Lett. 95 (113309) (2009) 1–3.
[39] K. DeLong, K. Rochford, G. Stegeman, Appl. Phys. Lett. 55 (2017) 1822–1830.
[40] M. Sheik-Bahae, A. Said, T. Wei, D. Hagan, E. Van Stryland, J. Quant. Econ. 26 (1990) 760–769.